Chinese Chemical Letters 36 (2025) 110379

Contents lists available at ScienceDirect

Chinese Chemical Letters

journal homepage: www.elsevier.com/locate/cclet

Electrochemical imaging uncovers the heterogeneity of HER activity by sulfur vacancies in molybdenum disulfide monolayer

Xiaoli Deng[a,1], Xiangchao Lu[b,1], Yang Cao[b,*], Qianjin Chen[a,*]

[a] Key Laboratory of Science and Technology of Eco-Textile, Ministry of Education, College of Chemistry and Chemical Engineering, Donghua University, Shanghai 201620, China

[b] State Key Laboratory of Physical Chemistry of Solid Surfaces, Collaborative Innovation Center of Chemistry for Energy Materials (iChEM), College of Chemistry and Chemical Engineering, Xiamen University, Xiamen 361005, China

ARTICLE INFO

Article history:
Received 8 April 2024
Revised 29 July 2024
Accepted 27 August 2024
Available online 29 August 2024

Keywords:
Nanoelectrochemistry
Scanning electrochemical cell microscopy
MoS_2 monolayers
Hydrogen evolution reaction
Sulfur vacancy

ABSTRACT

Engineering of sulfur vacancies on the basal plane of molybdenum disulfide (MoS_2) may provide effective way to promote the catalytic activity. Although the sulfur vacancy density has previously been correlated with catalytic activity, direct evidence that vacancies create surfaces with enhanced electrocatalytic activity is still lacking. Here, we used a combination of scanning electrochemical cell microscopy (SECCM) with submicrometer resolution and photoluminescence imaging to show that sulfur vacancies in monolayer MoS_2 microflakes lead to significant spatial heterogeneity in the electrochemical hydrogen evolution reaction (HER) activity. Specifically, colocated multi-microscopy unveils that regions with superior HER activity are associated with sulfur vacancy defects. As the vacancy density increases, the triangular flakes display significantly enhanced and spatially uniformly distributed electrocatalytic activity. Our multi-microscopic imaging approach using SECCM convincingly highlights the spatial heterogeneity of electrocatalytic activity across monolayer MoS_2 by sulfur vacancy engineering.

Transition-metal dichalcogenides, especially molybdenum disulfide (MoS_2), have been extensively investigated as an attractive catalyst for the electrochemical hydrogen evolution reaction (HER) [1,2]. Tremendous of work has been devoted to understanding the structure-activity relationship and optimizing the catalytic performance. It has been well acknowledged that the edge sites are active while the basal plane is relatively inert towards the electrochemical H_2 evolution [3,4]. Various strategies such as strain [5], doping [6], phase engineering [1,7], and heterostructures [8] have been developed to modulate the electronic structure and improve the catalytic activity of MoS_2 basal plane. Sulfur vacancy has been recognized as a key defect type that can dramatically perturb the local density of states and create additional energy states between Femi level, thus could effectively improve the catalytic activity [9-11]. Although many studies demonstrate the effect of sulfur vacancy concentration on the electrochemical and chemical catalysis [12,13], thorough understanding of the sulfur vacancy dependence requires spatially resolved measurements.

Several techniques have been employed for the local probing of electrocatalytic activity across 2D materials surface. The on-chip electrocatalytic microdevice platform, where the region of interest can be selectively exposed to electrolyte solution, allows high-precision and targeted local electrochemical measurement on single MoS_2 nanosheet level [14,15]. However, due to the sophisticated fabrication processes and a series of issues (*e.g.*, polymer passivation layer, current leakage), large cell-to-cell variations in measurements have been observed [16]. Other approaches such as scanning electrochemical microscopy (SECM) [17], super-resolution fluorescence microscopy (FL) [18], electrochemiluminescence microscopy (ECL) [19], and plasmonic imaging [20] offers high spatial/temporal resolution in detecting catalytic reaction across single catalysts. However, FL and ECL optical approaches are limited to fluorogenic reactions or that emit light. Label-free optical imaging method lacks the selectivity to recognize contribution from the intrinsic catalytic reaction. In all of the above methods, the effect of enhanced mass transport at perimeter (specific structures such as corners and edges) can be nontrivial, causing possible misidentification of the active sites.

Scanning electrochemical cell microscopy (SECCM), an emerging powerful technique that uses a glass nanopipette filled with electrolyte to scan across surfaces of interest, can resolve the fundamentals of various electrochemical processes with a high spa-

* Corresponding authors.
E-mail addresses: yangcao@xmu.edu.cn (Y. Cao), qianjinchen@dhu.edu.cn (Q. Chen).
[1] These authors contributed equally to this work.

https://doi.org/10.1016/j.cclet.2024.110379
1001-8417/

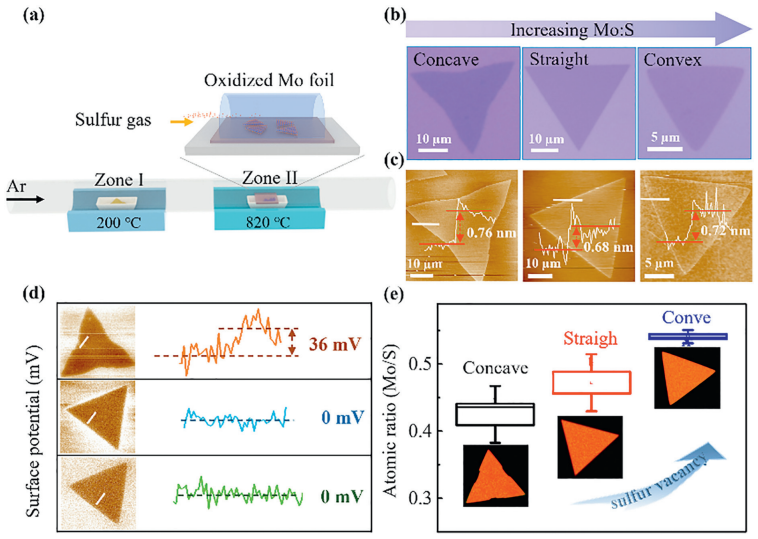

Fig. 1. Controllable growth and characterization of monolayer MoS_2 flakes on SiO_2/Si substrate. (a) CVD growth schematic of monolayer MoS_2 flakes. (b) Optical images, (c) atomic force microscopy topological images and height lines, (d) KPFM surface potential images and line profiles, (e) AES element (Mo and S) image and atom ratio (Mo/S) of the synthesized concave, straight and convex triangular monolayer MoS_2 flakes.

tial resolution [21,22], Importantly, SECCM is especially appropriate to reveal the mechanistic insights into the structure-property (activity) relationships across heterogeneous surfaces of 2D materials, such as graphene [23-25], MoS_2 [26-28], WSe_2 [29], Mexene [30], and others [31,32]. In this study, we comprehensively explore the electrochemical hydrogen evolution reaction across monolayer MoS_2 in the form of triangular microflakes with regulated sulfur vacancy using SECCM approach. Nanoscale inhomogeneity of electrocatalytic activity is clearly demonstrated. Characterization of kelvin probe force microscope (KPFM) and photoluminescence (PL) imaging on identical microflakes and regions elucidate the local electronic structures, unravelling the unambiguous correlation between catalytic activity and local sulfur vacancy defects. This study demonstrates the power of correlative co-located SECCM approach for understanding the spatial heterogeneity of electrocatalytic reaction at sub- transition-metal dichalcogenides flakes.

Large area high-quality crystals of monolayer 2H-MoS_2 were grown on a SiO_2/Si substrate by atmospheric pressure chemical vapor deposition (CVD) with oxidized Mo foil and S precursors as illustrated in Fig. 1a (details in section S1 in Supporting information) [33,34]. By precisely controlling the stoichiometry (Mo:S) during synthesis, triangular MoS_2 flakes with regulated sulfur vacancy density can be obtained and three different shapes from concave to straight and convex equilateral triangles with typical size of tens of micrometers are displayed in the optical images of Fig. 1b. Atomic force microscopy (AFM) topological images identify that the concave, straight, and convex triangular flakes have typical thicknesses of 0.76, 0.68, and 0.72 nm, respectively (white line in Fig. 1c), in accordance with the characteristic of monolayer MoS_2 [34].

The electronic structure of monolayer MoS_2 flakes is characterized by KPFM [35], where the surface potentials obtained are not calibrated with respect to the tip. Fig. 1d illustrates the easily distinguishable surface potential on MoS_2 samples from the SiO_2/Si substrate. The line profile shows that the surface potential across the straight and convex triangular flakes is relatively uniform, consistent with recent results of uniform electronic properties across straight triangular CVD-grown monolayer MoS_2 flakes [36,37]. In contrast, spatial heterogeneity in surface potential across the concave triangular flakes is demonstrated. Previously, this in-plane surface potential variances in single crystalline flakes is ascribed to the heterogeneous distribution of local defects [38,39] or strain [40]. Auger electron spectroscopy (AES) is employed to analyze the chemical distribution across MoS_2 microflakes [39,41]. The spectra and element map of Mo and S, associated with scanning electron microscope (SEM) images, are presented in Figs. S1–S4 (Supporting information), indictive of uniform atomic distribution [39]. Further atomic concentration analysis over different samples reveals that the Mo:S ratio increases from 0.43 to 0.47 and 0.54 with a significant decrease in sulfur content, as the flake morphology evolves from concave to straight and further to convex triangle (Fig. 1e). Such tendency of sulfur-deficiency in MoS_2 agrees well with the afore-mentioned stoichiometry control during CVD synthesis and suggests the variations in sulfur vacancy concentration of the three different shaped MoS_2 flakes.

Considering all the three types of MoS_2 flakes have identical compositions and there is no elastic strain applied in the course of experiment, we speculate that the non-uniform surface potential from KPFM image of the concave MoS_2 flake is attributed to the heterogenous distribution of defects. Extensive previous aberration-corrected scanning transmission electron microscopy studies suggest that the sulfur vacancies are the predominant point defects in pristine CVD-grown monolayer MoS_2 [39,42-44]. Based on the results of KPFM and AES, we conclude that as the morphology changes from concave to straight and further to convex triangle, the sulfur vacancy defects concentration significantly increases. Meanwhile, as the vacancy concentration increases, its spatial distribution across the microflakes changes from inhomogeneous to relatively uniform. This conclusion can be validated from the spatially resolved photoluminescence observations, which will be discussed later. In a nutshell, the different sulfur vacancy concentrations and spatial distributions make the three MoS_2 triangular flakes excellent candidates for understanding the spatial heterogeneities in electrocatalytic HER.

After characterization, the MoS_2 monolayers were carefully placed on a catalytically inert substrate using a wet etching transfer method assisted by PMMA, as detailed in section 2.1 in Supporting information [45]. Considering previous electrochemical microscopy of two dimensional materials [23,27] and supporting substrates effect on the HER of MoS_2 [46], atomically flat Ti thin layer was deposited on flat quart glass by electron-beam lithography to avoid possible local strain (Figs. S5 and S6 in Supporting information). Localized electrochemical measurement of HER across MoS_2 monolayers were performed using SECCM approach and the configuration is illustrated in Fig. 2 [47-49]. A single-

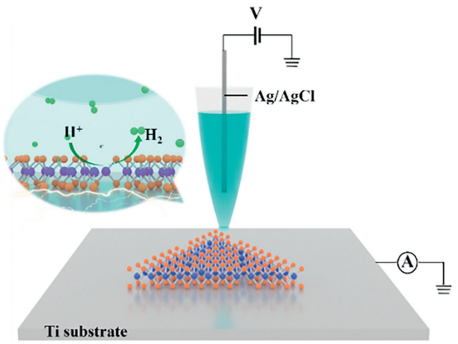

Fig. 2. Scheme of the scanning electrochemical cell microscopy study of hydrogen evolution reaction across a monolayer MoS_2 microflake on Ti substrate. The inset shows the hydrogen evolution reaction occurring at a sulfur vacancy defect.

barrel glass nanopipette with a tip opening radius of ~100 nm (Fig. S7 in Supporting information), filled with 10 mmol/L $HClO_4$ aqueous solution as electrolyte and inserted with an Ag/AgCl wire as the quasi-reference and counter electrode (QRCE) is used as the scanning probe. Variances in glass nanopipette geometry is carefully examined by the ionic conductance measurement [50], and nanopipettes with similar ionic current responses are chosen for experiments (Fig. S8 in Supporting information), ensuring the reliability of local electrochemical quantification. The position of the nanopipette is controlled by a piezoelectric motor in the z direction to slowly approach the substrate. Once the meniscus contacts the substrate, a nanometer-sized electrochemical droplet cell is established and consequent electrochemical measurement such as linear sweep voltammetry (LSV) for HER on the sample surface will be performed. The substrate confined by the meniscus droplet serves as the working electrode. Electrochemical imaging is obtained by using a repetitive "hopping" mode scanning across the sample surface (Fig. S9 in Supporting information) and the step distances vary from 500 nm to 2 μm depending the lateral dimension of individual MoS_2 microflakes. The spatial resolution in our SECCM study is limited by the size of the nanopipette (~200 nm diameter) as well as the hopping distance between each spot. Due to the speed limit of pipette approaching, the arrays for 30×30 pixels typically take ~120 min. The current density is obtained by picking up the current from LSV and divided by an electrode area [23,51], as estimated from SEM images of the post-SECCM footprints with additional electrolyte salt introduced. The observed consistent in droplet footprint size in Fig. S10 (Supporting information) suggests the reproducibility of droplet wetting during electrochemical mapping and the reliability of quantification of current density. It should be noted that due to the *iR* drop in SECCM, such current density value from nanoscale electrochemical measurement is not comparable to that obtained from macroscopic measurement [52].

Typical SECCM results obtained at individual monolayer MoS_2 flakes consist of correlated optical image, electrochemical HER current density image, and photoluminescence image. Figs. 3a–c show the optical images of the concave, straight, and convex triangular MoS_2 flakes before SECCM experiments. The HER current density image at –1.20 V *vs.* Ag/AgCl across the corresponding MoS_2 flakes are demonstrated in Figs. 3d–f. It is found that current across MoS_2 samples shows higher magnitude relative to the Ti substrate and the edge positions display comparable activity with the basal plane for all the three flakes. This observation of equivalent activity at edge and basal plane is in line with recent report of heterogeneous electron transfer on CVD-grown concave triangular monolayer MoS_2 using bright field optical imaging [53]. Meanwhile, previous local electrochemical measurement on bulk MoS_2 surfaces found highly superior HER activity at edge positions with tens of MoS_2 layers, but only slightly superior (130%) at edge positions with a few (~2–3) layers [26]. We expect that the unobserved superior activity at the edges in current study is likely due to the tiny proportion of the edges within the total area encapsulated by the meniscus droplet. Nevertheless, the spatial resolved electrochemical HER activity within the MoS_2 basal plane can be revealed. While the concave triangle exhibits uneven distribution of catalytic activity (Fig. 3d), the straight and convex triangular samples display relatively uniform distribution of activity (Figs. 3e and f). Additional HER current images at different potentials (–0.9 and –1.1 V *vs.* Ag/AgCl) of the three different flakes are presented in Fig. S11 (Supporting information), demonstrating the consistent heterogeneity of catalytic activity on concave triangular monolayer MoS_2 flakes.

To understand the heterogeneity of HER activity, spatially resolved photoluminescence imaging was performed across the same MoS_2 flake/region of the SECCM measurements [54]. Figs. 3g–i shows the corresponding photoluminescence intensity map at 1.82 eV across individual flakes under a laser wavelength of 532 nm. Interestingly, it is observed that the straight and convex triangular flakes exhibit relatively uniform emission intensity distribution (Figs. 3h and i) while the concave triangular sample displays noticeable in-plane emission intensity heterogeneity (Fig. 3g). This observation is fully consistent with the surface potential distribution as earlier revealed by KPFM in Fig. 1d. Previous optoelectronic studies of pristine CVD-grown monolayer MoS_2 reported similar inhomogeneity within concave triangular microflakes [41,55], and relative homogeneity within straight triangular microflakes [55]. Since strain effect and doping can be excluded in our study, the variations of in-plane emission intensity can be ascribed to the uneven distribution of sulfur vacancy defects. In Figs. 3g–i, an overall reduction of PL intensity is observed with increasing sulfur vacancy concentration, similar to previous works on sulfur vacancy engineering [41,44]. Region with significantly high emission intensity, indictive of low electron concentration, as noted by the arrow in Fig. 3g, displays low HER activity in Fig. 3d. Finally, we discuss the overall local HER activity for the three different samples. Figs. 3j and k display the histograms of the current density at –1.2 V *vs.* Ag/AgCl and overpotential at a current density of –30 mA/cm^2, respectively, over three different MoS_2 flakes. It is clearly demonstrated that the convex triangular flakes with highest sulfur vacancy concentration shows significantly (~7 times) higher HER activity as compared to the concave triangular flakes. This phenomenon of the sulfur vacancy effect on HER activity is fully consistent with previous results from macroscopic measurement of MoS_2 nanosheets [9,13].

To fully validate the spatial correlation between the sulfur vacancy defects and HER activity, larger area concave MoS_2 microflakes were prepared for further examination using identical scanning nanopipette probe. As presented in Fig. 4, two distinct regions of a ~70 μm concave triangle MoS_2 flake are independently mapped for electrochemical HER. It is observed that corner A exhibits significantly higher HER activity relative to corner B (Fig. 4b). Presentative current responses at different positions are shown in Fig. 4d. The current density at –1.2 V *vs.* Ag/AgCl at position 2 is as high as 380 mA/cm^2, which is about 3 times of that at position 1 (126 mA/cm^2). Fig. 4e summarizes the distributions of HER current density from individual isolated nanoscale electrochemical measurements in corners A and B. Two peaks located around 105 and 290 mA/cm^2, respectively, are observed in corner A and only one peak around 70 mA/cm^2 is observed in corner B. Parallel analysis of overpotential at a constant current density (–30 mA/cm^2) shows similar result of superior activity at corner A (Fig. S14 in Supporting information), thus confirming the significant inhomogeneity in HER activity across the concave triangular flakes. Importantly, Fig. 4c shows the spatially resolved photoluminescence

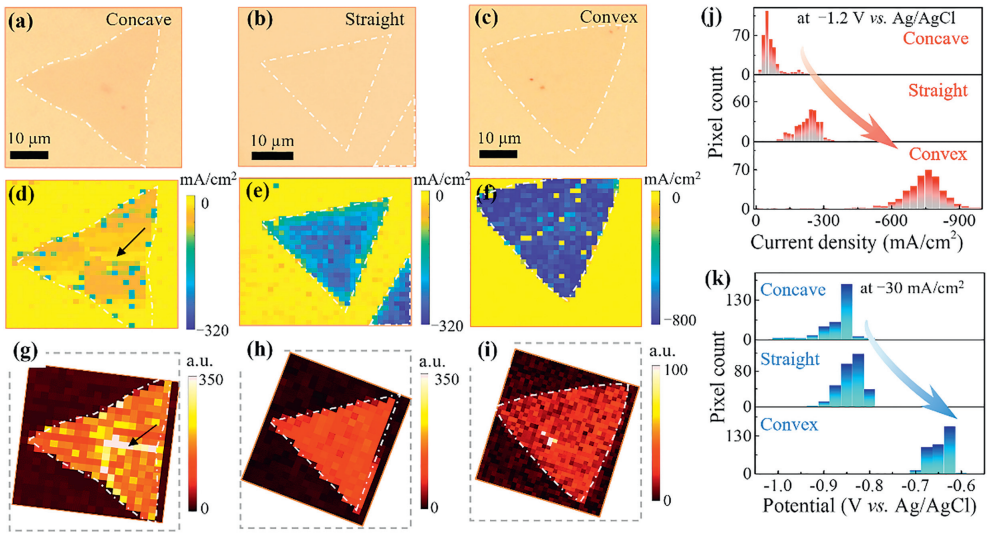

Fig. 3. Correlative SECCM and photoluminescence study of HER on monolayer MoS_2 flakes. (a-c) Optical images, (d-f) electrochemical HER current density maps at −1.2 V *vs.* Ag/AgCl, (g-i) photoluminescence intensity images at 1.82 eV across a concave, straight and convex triangular monolayer MoS_2 flakes on Ti substrate. In the SECCM experiment, a solution of 10 mmol/L $HClO_4$ was used as the supporting electrolyte. The potential was initiated at −0.4 V and swept from −0.4 V to −1.3 V *vs.* Ag/AgCl at a scan rate of 1 V/s. (j) The histogram of HER current density at −1.2 V *vs.* Ag/AgCl, and (k) histogram of potential at −30 mA/cm² from individual local microscopic electrochemical measurements over the three MoS_2 flakes in d-f. The yellow pixels in (d, e, f) over the MoS_2 samples correspond to defects from the SECCM measurement, where droplet contacts were not established.

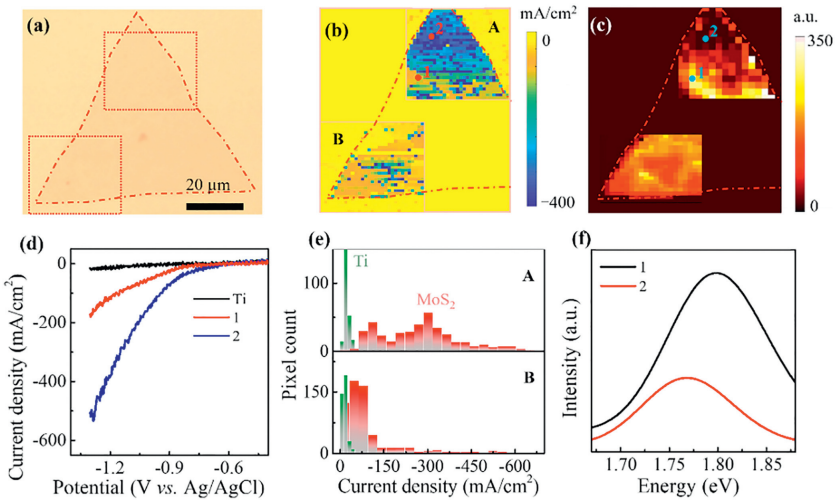

Fig. 4. Correlative (a) optical image, (b) SECCM HER current density image, and (c) photoluminescence intensity image at 1.82 eV of a ~70 μm concave triangular monolayer MoS_2 flake. (d) Typical HER current responses with 1 V/s at locations as indicated in (b). (e) Histogram of HER current density at −1.2 *vs.* Ag/AgCl for Ti substrate (green) and MoS_2 sample (red). (f) Typical photoluminescence spectra at locations as indicated in (c).

image of the same MoS_2 concave triangular flake, where distinct variations in photoluminescence intensity between corners A and B is explicitly demonstrated. The photoluminescence spectra at position 2 shows a great decrease in intensity and low bandgap shift compared with position 1 (Fig. 4f), indicative of the presence of more local sulfur vacancy defects [56]. After examining more co-located microscopy of additional MoS_2 microflakes (Figs. S15-S18 in Supporting information), it is decisively to conclude that the local superior HER activity is correlated with sulfur vacancy defects.

In summary, different from the existing three-electrode ensemble system with a macroscopic composite electrode and the on-chip electrochemical microdevices, the heterogeneity in electrocatalytic hydrogen evolution reaction across CVD-grown monolayer MoS_2 flakes was spatially resolved by scanning electrochemical cell microscopy. Large area single-crystalline triangular microflakes with deliberately regulated sulfur vacancies concentration were examined. The local structure and sulfur vacancies on the basal plane was revealed by a series of co-located microscopy including kelvin probe force microscope, auger electron spectroscopy mapping and photoluminescence imaging. From an unprecedented correlative SECCM and photoluminescence imaging of individual monolayer MoS_2 microflakes, the intrinsic electrocatalytic activity is correlated with local vacancy structures. Significant nanoscale inhomogeneity in electrochemical HER activity is explicitly observed on concave triangular MoS_2 flakes with low vacancy density. In contrast, the straight and convex triangular MoS_2 flakes with high vacancy density, exhibit a relatively uniform HER activity across the sample. Compared with recent SECCM study on defects in MoS_2 flakes [57-59], our work features the correlative SECCM and PL images for MoS_2 samples with deliberately regulated sulfur vacancy density. Direct and persuasive evidence for the enhanced catalytic activity by sulfur vacancy is demonstrated. The strategy can be applicable for the unambiguous understanding of more structure-function relationship of other transition-metal dichalcogenides materials.

Declaration of competing interest

The authors declare that they have no known competing financial interests or personal relationships that could have appeared to influence the work reported in this paper.

CRediT authorship contribution statement

Xiaoli Deng: Writing – original draft, Methodology, Investigation, Data curation, Conceptualization. **Xiangchao Lu:** Writing – original draft, Methodology, Investigation, Formal analysis, Data curation. **Yang Cao:** Writing – review & editing, Supervision, Funding acquisition. **Qianjin Chen:** Writing – review & editing, Supervision, Funding acquisition, Conceptualization.

Acknowledgments

We acknowledge the Fundamental Research Funds for the Central Universities (Nos. 2232023G-04 and 20720210009), National Natural Science Foundation of China (Nos. NSFC-22274019 and 92163103) and National Key R&D Program of China (No. 2022YFA1505200) for financial support. Q. Chen is sponsored by National Ten Thousand Talent Program for young top-notch talent.

Supplementary materials

Supplementary material associated with this article can be found, in the online version, at doi:10.1016/j.cclet.2024.110379.

References

[1] Y. Yin, J. Han, Y. Zhang, et al., J. Am. Chem. Soc. 138 (2016) 7965–7972.
[2] Q. Fu, J. Han, X. Wang, et al., Adv. Mater. 33 (2021) 1907818.
[3] T.F. Jaramillo, K.P. Jørgensen, J. Bonde, et al., Science 317 (2007) 100–102.
[4] J. Zhang, J. Wu, H. Guo, et al., Adv. Mater. 29 (2017) 1701955.
[5] H. Li, C. Tsai, A.L. Koh, et al., Nat. Mater. 15 (2016) 48–53.
[6] J. Deng, H. Li, J. Xiao, et al., Energy Environ. Sci 8 (2015) 1594–1601.
[7] J. Zhu, Z.C. Wang, H. Dai, et al., Nat. Commun. 10 (2019) 1348.
[8] G. Shao, Y. Lu, J. Hong, et al., Adv. Sci. 7 (2020) 2002172.
[9] P. Man, S. Jiang, K.H. Leung, et al., Adv. Mater. 36 (2024) 2304808.
[10] C. Tsai, H. Li, S. Park, et al., Nat. Commun. 8 (2017) 15113.
[11] X. Wang, Y. Zhang, H. Si, et al., J. Am. Chem. Soc. 142 (2020) 4298–4308.
[12] G. Ye, Y. Gong, J. Lin, et al., Nano Lett. 16 (2016) 1097–1103.
[13] L. Li, Z. Qin, L. Ries, et al., ACS Nano 13 (2019) 6824–6834.
[14] W. Wang, J. Qi, Z. Wu, et al., Nat. Protoc. 18 (2023) 2891–2926.
[15] H. Yang, Q. He, Y. Liu, et al., Chem. Soc. Rev. 49 (2020) 2916–2936.
[16] H. Xia, X. Sang, Z. Shu, et al., Nat. Commun. 14 (2023) 6838.
[17] H. Li, M. Du, M.J. Mleczko, et al., J. Am. Chem. Soc. 138 (2016) 5123–5129.
[18] N.M. Andoy, X. Zhou, E. Choudhary, et al., J. Am. Chem. Soc. 135 (2013) 1845–1852.
[19] M.M. Chen, W. Zhao, M.J. Zhu, et al., Chem. Sci. 10 (2019) 4141–4147.
[20] X. Zhao, X.L. Zhou, S.Y. Yang, et al., Nat. Commun. 13 (2022) 7869.
[21] X. Xu, D. Valavanis, P. Ciocci, et al., Anal. Chem. 95 (2023) 319–356.
[22] D. Martín Yerga, P.R. Unwin, D. Valavanis, X. Xu, Curr. Opin. Electrochem. 42 (2023) 101405.
[23] D.Q. Liu, M. Kang, D. Perry, et al., Nat. Commun. 12 (2021) 7110.
[24] Y. Yu, K. Zhang, H. Parks, et al., Nat. Chem. 14 (2022) 267–273.
[25] O.J. Wahab, E. Daviddi, B. Xin, et al., Nature 620 (2023) 782–786.
[26] C.L. Bentley, M. Kang, F.M. Maddar, et al., Chem. Sci. 8 (2017) 6583–6593.
[27] Y. Takahashi, Y. Kobayashi, Z. Wang, et al., Angew. Chem. Int. Ed. 59 (2020) 3601–3608.
[28] H. Zheng, M. Li, J. Chen, et al., Chin. Chem. Lett. 33 (2022) 1450–1454.
[29] J.W. Hill, C.M. Hill, Chem. Sci. 12 (2021) 5102–5112.
[30] M. Brunet Cabré, D. Spurling, P. Martinuz, et al., Nat. Commun. 14 (2023) 374.
[31] J.T. Mefford, A.R. Akbashev, M. Kang, et al., Nature 593 (2021) 67–73.
[32] Y. Peng, C. Gao, X. Deng, et al., Anal. Chem. 95 (2023) 11657–11663.
[33] J. Zhang, F. Wang, V.B. Shenoy, et al., Mater. Today 40 (2020) 132–139.
[34] S. Najmaei, Z. Liu, W. Zhou, et al., Nat. Mater. 12 (2013) 754–759.
[35] W. Melitz, J. Shen, A.C. Kummel, S. Lee, Surf. Sci. Rep. 66 (2011) 1–27.
[36] W. Yim, V.T. Nguyen, Q.T. Phung, et al., ACS Appl. Mater. Interfaces. 14 (2022) 26295–26302.
[37] H.Y. Du, Y.F. Huang, D. Wong, et al., Nat. Commun. 12 (2021) 1321.
[38] X. Wang, J. Dan, Z. Hu, et al., Chem. Mater. 31 (2019) 7970–7978.
[39] L. Gao, Q. Liao, X. Zhang, et al., Adv. Mater. 32 (2020) 1906646.
[40] A.C. De Palma, X. Peng, S. Arash, et al., Nano Lett. 24 (2024) 1835–1842.
[41] J. Gao, B. Li, J. Tan, et al., ACS Nano 10 (2016) 2628–2635.
[42] J. Hong, Z. Hu, M. Probert, et al., Nat. Commun. 6 (2015) 6293.
[43] W. Zhou, X. Zou, S. Najmaei, et al., Nano Lett. 13 (2013) 2615–2622.
[44] J. Xiao, K. Chen, X. Zhang, et al., Small Methods 7 (2023) 2300611.
[45] Y. Gong, J. Lin, X. Wang, et al., Nat. Mater. 13 (2014) 1135–1142.
[46] G. Li, Z. Chen, Y. Li, et al., ACS Nano 14 (2020) 1707–1714.
[47] J. Zhao, M. Wang, Y. Peng, et al., Angew. Chem. Int. Ed. 62 (2023) e202304424.
[48] X. Deng, Y. Shan, X. Meng, et al., Proc. Natl. Acad. Sci. U. S. A. 119 (2022) e2205827119.
[49] Y. Shan, X. Deng, X. Lu, et al., Chin. Chem. Lett. 33 (2022) 5158–5161.
[50] D. Perry, D. Momotenko, R.A. Lazenby, et al., Anal. Chem. 88 (2016) 5523–5530.
[51] R.G. Mariano, M. Kang, O.J. Wahab, et al., Nat. Mater. 20 (2021) 1000–1006.
[52] B. Blount, G. Juarez, Y. Wang, H. Ren, Faraday Discuss. 233 (2022) 149–162.
[53] J. Ma, Z. Wang, B. Jiang, et al., Angew. Chem. Int. Ed. 62 (2023) e202305846.
[54] Z. Liu, M. Amani, S. Najmaei, et al., Nat. Commun. 5 (2014) 5246.
[55] I.S. Kim, V.K. Sangwan, D. Jariwala, et al., ACS Nano 8 (2014) 10551–10558.
[56] Y. Zhu, J. Lim, Z. Zhang, et al., ACS Nano 17 (2023) 13545–13553.
[57] M.B. Cabré, A.E. Paiva, M. Velický, et al., J. Phys. Chem. C 126 (2022) 11636–11641.
[58] C.L. Bentley, L.F. Gaudin, M. Kang, Chem. Commun. 59 (2023) 2287–2290.
[59] I.H. Abidi, S.P. Giridhar, J.O. Tollerud, et al., Adv. Funct. Mater. 34 (2024) 2402402.